

Spray Icing Simulation and Anti-icing Optimization for Ship Intake Grilles in Cold Environments

FENG Huiying¹, PAN Tao^{1*}, LOU Yanxia², BU Xueqin²

1. Systems Engineering Research Institute, CSSC, Beijing 100094, P. R. China;

2. School of Aeronautic Science and Engineering, Beihang University, Beijing 100191, P. R. China

(Received 15 January 2025; revised 1 March 2025; accepted 2 March 2025)

Abstract: This study addresses the issue of spray icing on the air intake grilles of ship power systems in cold maritime environments. Through numerical simulation methods, the influence of environmental parameters on icing characteristics is revealed, and an energy-efficient zoned electric heating anti-icing strategy is proposed. A three-dimensional grille model is constructed to systematically analyze the effects of environmental temperature (from $-20\text{ }^{\circ}\text{C}$ to $-4\text{ }^{\circ}\text{C}$), droplet diameter (from $50\text{ }\mu\text{m}$ to $500\text{ }\mu\text{m}$), and liquid water content (from 0.5 g/m^3 to 8 g/m^3) on icing rates and blockage of the flow channel. The results indicate that low temperature and high liquid water content significantly exacerbate icing. Under the condition of an environmental temperature of $-20\text{ }^{\circ}\text{C}$, droplet diameter of $500\text{ }\mu\text{m}$, and liquid water content of 8 g/m^3 , the flow channel blockage ratio reaches 30.95% within 10 min. Additionally, as droplet diameter increases, the droplet impingement and icing regions become more concentrated toward the leading edge of blades. To mitigate grille icing in cold environments, an electric heating film configuration is employed for thermal protection. Optimization of the heating strategy reveals that the zoned heating approach, compared to the initial uniform heating scheme, effectively homogenizes surface temperature distribution while reducing total power consumption by 37.47% . This study validates the engineering applicability of the zoned electric heating anti/de-icing strategy, providing theoretical and technical support for the design of anti-icing systems in ship power systems operating in cold maritime regions.

Key words: ship intake grilles; icing characteristics; maritime environment; flow channel blockage; zoned electric heating strategy

CLC number: U661 **Document code:** A **Article ID:** 1005-1120(2025)02-0226-12

0 Introduction

With the increasing frequency of global maritime activities, the safety of ships navigating in cold regions has garnered significant attention. When sailing for extended periods in cold environments, ships are exposed to rain, snow, and seawater spray, which can rapidly freeze on ship surfaces. Ship icing primarily manifests in two forms: Seawater spray icing and atmospheric icing. The former mainly consists of saline ice formed from seawater and the latter primarily involves freshwater ice. According to statistical studies on icing incidents involving numer-

ous fishing vessels^[1], seawater spray icing accounts for 89.8% of all icing events. Seawater spray icing occurs when droplets in the air collide with the ship and subsequently freeze. This phenomenon can be further categorized into impact spray and wind-driven spray. In fact, 90% of icing incidents are attributed to impact spray generated by the interaction between waves and the ship. Therefore, this study focuses on the icing phenomenon caused by impact-generated seawater spray.

The formation of spray at the ship's bow is complex (Fig.1) and is influenced by numerous factors,

*Corresponding author, E-mail address: iampantao@163.com.

How to cite this article: FENG Huiying, PAN Tao, LOU Yanxia, et al. Spray icing simulation and anti-icing optimization for ship intake grilles in cold environments[J]. Transactions of Nanjing University of Aeronautics and Astronautics, 2025, 42(2):226-237.

<http://dx.doi.org/10.16356/j.1005-1120.2025.02.007>

including environmental parameters such as wind speed, air temperature, droplet temperature, droplet size, relative humidity and wave speed. Additionally, ship-specific characteristics, such as vessel size, hull shape, speed, and heading, also significantly influence the icing process. Through a comprehensive analysis of these parameters, a thorough understanding of spray icing mechanisms can be achieved. Generally, seawater spray icing can be observed within specific ranges: Wind speeds of 9—55 m/s, air temperatures of $-29\text{ }^{\circ}\text{C}$ to $-2\text{ }^{\circ}\text{C}$ ^[2-3], and seawater surface temperatures of $-1.8\text{ }^{\circ}\text{C}$ to $+6\text{ }^{\circ}\text{C}$ ^[4].

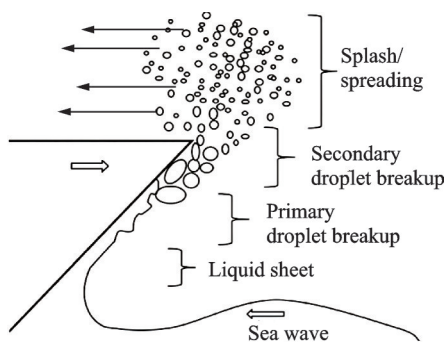


Fig.1 Schematic diagram of impact spray formation

Over the past few decades, domestic and foreign scholars have accumulated and summarized extensive experimental data on ship icing. Early research primarily focused on atmospheric and marine spray icing experiments, combined with semi-quantitative analysis, to predict and evaluate icing rates. Sawada^[5] created a relationship diagram between ship icing with air temperature and wind speed based on data from Japanese patrol boats and fishing vessels. Mertins^[6] developed icing charts for German trawlers based on 400 field observations in the northeastern Atlantic. Malsh et al.^[7] conducted icing tests on new turbine intake louvers of U.S. navy destroyers, while Ryerson et al.^[8-9] published a database on seawater spray and ice accumulation for Coast Guard cutters navigating the North Pacific and Bering Sea. These studies have provided crucial theoretical and data support for the prediction and prevention of ship icing.

At theoretical and simulation level, research spans from fundamental physical models to numeri-

cal simulations of complex structures. Makkonen^[10] investigated marine spray icing on unheated horizontal cylinders through experiments and model analysis, finding that the model aligned well with experimental data in short-term tests but showed significant deviations in long-term tests. Paul Zakrzewski et al.^[11] established a seawater spray model for medium-sized fishing vessels, analyzing the effects of wind speed, ship speed, and heading on the height of splashed seawater. The study noted that the maximum height of seawater spray occurred when the angle between the ship's heading and the wind vector was between 110° and 120° . Blackmore et al.^[12] proposed two heuristic models for spray icing, namely the supercooling model and the nucleation model. They calculated the marine spray icing rates under these two conditions and validated the effectiveness of the models using experimental data. Kulyakhtin et al.^[13] developed a three-dimensional time-dependent model using the MARICE solver, employing empirical formulas to determine the flow rate of splashed seawater and simulating marine spray icing on drilling platforms (as shown in Fig.2). Kulyakhtin et al.^[14] introduced a new method to calculate periodic spray icing, incorporating the thermal conductivity of ice and its substrate, with the model showing less than a 25% deviation from experimental results. Samuelsen et al.^[15] developed the MINCOG model to predict icing on Norwegian Coast Guard vessels.

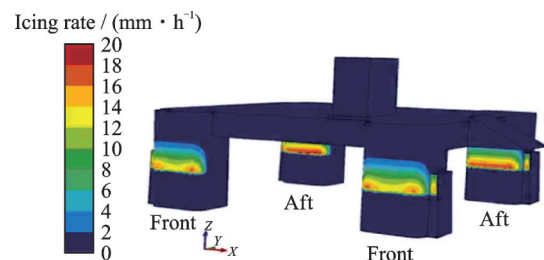


Fig.2 Icing rate on the West Hercules drilling platform under $t_a = -17\text{ }^{\circ}\text{C}$, $\phi = 90^{\circ}$, and $U_{10} = 33\text{ m/s}$ ^[13]

In 2023, Horjen^[16] extended the time-dependent two-dimensional sea spray icing model ICEMOD2.1. The first extension, called ICEMOD2.2, incorporates the calculation of heat conduction through the accreted ice. This quantity is derived

from the temperature distribution within the ice, which varies over time. The second extension, called ICEMOD2.3, integrates the combined effects of sea spray and snow. No other icing models have previously included this effect. In 2024, Deshpande et al.^[17] conducted experimental research on sea spray icing in the cold climate laboratory at Arctic University of Norway. The experiments focused on a flat plate, and the results indicated that wind speed and atmospheric temperature had the greatest impact on the icing rate.

Based on the current research status, it can be concluded that experimental and simulation analysis of spray icing have established a certain foundation. However, three-dimensional numerical simulation research of icing on grille surfaces remains insufficient, particularly with regard to the quantitative analysis of flow channel blockage caused by icing. Existing studies have predominantly focused on two-dimensional or simplified models, lacking in-depth exploration of ice distribution and its impact on flow characteristics in complex three-dimensional geometries. Furthermore, research on the quantitative relationship between icing rate and degree of flow channel blockage is relatively scarce.

Therefore, this paper will focus on the ship's air intake grille, constructing a three-dimensional simulation model. Through simulation methods, a quantitative analysis will be conducted to assess the icing rates under different meteorological conditions (such as temperature, liquid water content, and droplet diameter), as well as the blockage of flow channels. On this basis, the effectiveness of electric heating methods for anti-icing will be evaluated and optimized, culminating in the development of efficient and energy-saving anti-icing strategies. This work aims to provide theoretical support and technical guidance for the anti-icing design of ship intake grilles.

1 Model Description

The main focus of this study is the freezing of wind-driven sea spray, rather than the splashed sea water. Compared to sea water splashing, the liquid

water content in sea spray freezing is significantly lower. Therefore, the fundamental principles of icing on ship intake grilles are similar to those of aircraft icing, both involving the process of super-cooled water droplets impacting and freezing on solid surfaces. Parameters such as ambient temperature, droplet diameter, liquid water content (LWC), and airflow velocity significantly influence the icing rate and distribution. However, the diameter of seawater splash droplets is generally larger, and the impact efficiency and droplet trajectories may differ from those in aircraft icing. In this study, only the icing process caused by seawater spray impacting the grille surface is considered, without detailed simulation of the motion and heat transfer processes of droplets in the air. Therefore, by adjusting the droplet diameter distribution and impact efficiency according to different environmental parameters, a process similar to aircraft icing can be adopted to simulate the icing process on ship intake grilles.

To more accurately reflect the actual operational conditions of ships in cold maritime environments, a simulation model for icing on the surface of a ship's intake grille is established based on actual physical models. Through simulation methods, the quantitative effects of various factors, such as ambient temperature, liquid water content, and droplet diameter, on spray icing are systematically considered.

1.1 Theoretical model

To conduct simulation calculations of the icing phenomenon on a grille surface, it is essential to thoroughly understand the theoretical models involved in the thermodynamic process. This primarily includes three components: Air flow field calculation, droplet impingement characteristics calculation, and icing calculation. Below, a brief theoretical model description is provided for each of these parts.

(1) Air flow field calculation

The fluid to be solved must satisfy three fundamental conservation laws: The law of conservation of mass, the law of conservation of momentum, and the law of conservation of energy. The govern-

ing equations are as follows.

The continuity equation is

$$\frac{\partial u_x}{\partial x} + \frac{\partial u_y}{\partial y} + \frac{\partial u_z}{\partial z} = 0 \quad (1)$$

where $\mathbf{u} = (u_x, u_y, u_z)$ represents the air velocities in three directions, respectively, measured in m/s.

The momentum conservation equation is

$$\frac{\partial \mathbf{u}}{\partial t} + (\mathbf{u} \cdot \nabla) \mathbf{u} = -\frac{1}{\rho} \nabla p + \frac{\mu}{\rho} \nabla^2 \mathbf{u} + \mathbf{g} \quad (2)$$

where p is the pressure and μ the dynamic viscosity.

The energy conservation equation is

$$\begin{cases} \frac{\partial T}{\partial t} + (\mathbf{u} \cdot \nabla) T = \alpha \nabla^2 T \\ \alpha = \frac{\kappa}{\rho c_p} \end{cases} \quad (3)$$

where T is the temperature, α the thermal diffusivity coefficient, κ the thermal conductivity coefficient, and c_p the specific heat capacity.

(2) Droplet impingement characteristics calculation

The motion trajectory of supercooled water droplets in the air and their impact on the surface of blades is a typical two-phase flow problem. Based on the Eulerian method, the droplets are treated as a continuous phase to calculate the droplet impact characteristics. The governing equations are as follows.

$$\begin{cases} \frac{\partial \alpha}{\partial t} + \nabla \cdot (\alpha \mathbf{V}_a) = 0 \\ \frac{\partial (\alpha \mathbf{V}_a)}{\partial t} + \nabla \cdot (\alpha \mathbf{V}_a \otimes \mathbf{V}_d) = \\ \frac{C_D Re_d}{24K} \alpha (\mathbf{V}_a - \mathbf{V}_d) + \alpha \left(1 - \frac{\rho_a}{\rho_d} \right) \frac{1}{Fr^2} \\ Re_d = \frac{\rho_a d \mathbf{V}_{a,\infty} \|\mathbf{V}_a - \mathbf{V}_d\|}{\mu_a} \\ C_D = \begin{cases} 24(1 + 0.15 Re_d^{0.687}) / Re_d & Re_d < 1000 \\ 0.44 & Re_d \geq 1000 \end{cases} \\ K = \frac{\rho_d d^2 \mathbf{V}_{a,\infty}}{19L_\infty \mu_a} \end{cases} \quad (4)$$

where α represents the volume fraction of supercooled water droplets, \mathbf{V}_a the velocity of air, \mathbf{V}_d the velocity of droplets, ρ_a the density of air, ρ_d the density of droplets, μ_a the dynamic viscosity of air, C_D the drag coefficient of droplets, Re_d the Reynolds number of droplets, d the droplet diameter, K the

inertia parameter, L_∞ the characteristic length, and Fr the Froude number.

(3) Icing calculation

The calculation for supercooled water droplets icing on the blade involves using thermodynamic analysis. This approach simulates the icing process on the surface of the grid blade by applying the conservation laws of heat and mass transfer. Due to shear stress, centrifugal force, or gravity, the film on the surface of blades may experience overflow. Depending on the thermodynamic conditions, a portion of the film may freeze, evaporate, or sublimate.

The governing equations are as follows

$$\begin{cases} \rho_f \left[\frac{\partial h_f}{\partial t} + \nabla \cdot (\mathbf{V}_f h_f) \right] = V_{rel} \cdot LWC \cdot \beta - \dot{m}_{evap} - \dot{m}_{ice} \\ \rho_f \left[\frac{\partial h_f c_f \tilde{T}_f}{\partial t} + \nabla \cdot (\mathbf{V}_f h_f c_f \tilde{T}_f) \right] = \left[c_f (\tilde{T}_\infty - \tilde{T}_f) + \frac{\|\mathbf{V}_d\|}{2} \right] \cdot \\ V_{rel} \cdot LWC \cdot \beta - L_{evap} \dot{m}_{evap} + (L_{fusion} c_s \tilde{T}) \dot{m}_{ice} + \\ \sigma \varepsilon (T_\infty^4 - T_f^4) - c_h (\tilde{T}_f - \tilde{T}_{ice,rec}) + Q_{anti-icing} \end{cases} \quad (5)$$

where the subscript of “f” represents the water film, \dot{m}_{evap} the instantaneous evaporation mass, \dot{m}_{ice} the instantaneous icing mass, and $Q_{anti-icing}$ the anti-icing heat flux; ρ_f , c_f , c_s , ε , σ , L_{evap} , and L_{fusion} represent physical properties of the fluid.

1.2 Geometric model of an intake grille

The configuration of the grille blade is illustrated in Fig.3, while the overall grille model is depicted in Fig.4. Considering both practical application scenarios and computational workload of simulations, a three-dimensional partial grille model is developed. The overall dimension of the model is 150 mm × 320 mm × 440 mm, comprising a total of seven blades. Appropriate blade spacing is ensured, with an adjacent blade spacing of 38 mm.

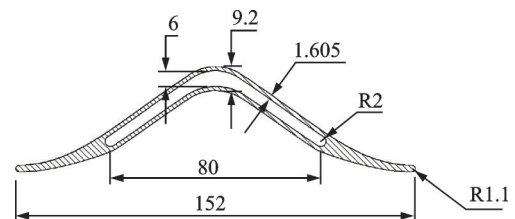


Fig.3 Geometric model of single blade

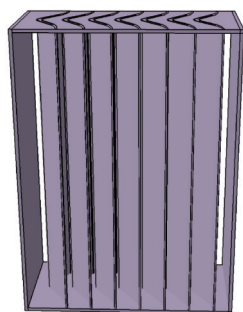
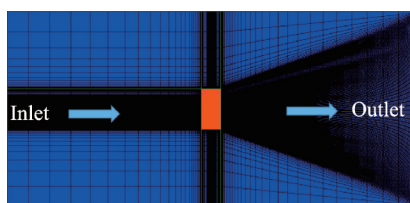


Fig.4 Geometric model of a partial intake grille

1.3 Meshing

Based on the grille model illustrated in Fig.4, a structured mesh for the external flow field is generated. A schematic diagram of the mesh is shown in Fig.5.



(a) Top view of external flow field mesh



(b) Detailed view of the mesh near the grille

Fig.5 Schematic diagrams of external flow field mesh

The solid surface mesh of the grille is also constructed using a structured grid, with a total mesh count of 1 615 200. The solid mesh of a cross-section of a single blade is shown in Fig.6.



Fig.6 Solid mesh of the blade

1.4 Simulation cases

Referring to the seawater spray icing database and typical wind speeds adopted in numerous studies by scholars, a wind speed of 10 m/s is selected as the representative value for this research. Based

on it, the effects of ambient temperature, median volume diameter (MVD) of droplets, and LWC on the icing phenomenon are investigated. Three typical ambient temperatures, four typical MVD values, and five typical LWC values are chosen. The specific cases are listed in Table 1.

Table 1 Cases for icing simulation

Ambient temperature/ $^{\circ}\text{C}$	MVD/ μm	LWC/ $(\text{g}\cdot\text{m}^{-3})$
-20, -12	50, 100	0.5, 1, 2
-4	200, 500	4, 8

2 Icing Analysis

This paper conducts thermodynamic calculations for icing on the surface of the ship's power intake grille, investigating variations in heat transfer characteristics, ice accretion rate, and freezing area under different temperatures, MVD values and liquid water contents. The icing simulation is conducted using commercial software FENSAP-ICE, a specialized tool designed for simulating and analyzing icing and its impact on aerodynamic performance.

To quantitatively investigate the impact of droplet diameter on icing formation on the grille surface, the droplet diameter of the incoming flow is assumed to be uniform. Additionally, since the influence of non-uniformity of airflow and droplet composition are neglected in this study, the physical properties of the fluid are assumed to be constant.

In addition, although the presence of salt in seawater affects freezing—specifically, the salt lowers the freezing point of water, causing seawater to freeze more slowly under the same low-temperature conditions. However, according to the literature reviewed, the influence of salinity on the freezing rate is relatively minor compared to environmental parameters such as wind speed and temperature^[17]. Therefore, in this study, the effect of salinity is temporarily not considered.

The icing calculation process is illustrated in Fig.7.

By setting the relative air velocity to 10 m/s and the pressure to 101 325 Pa, the flow field calcu-

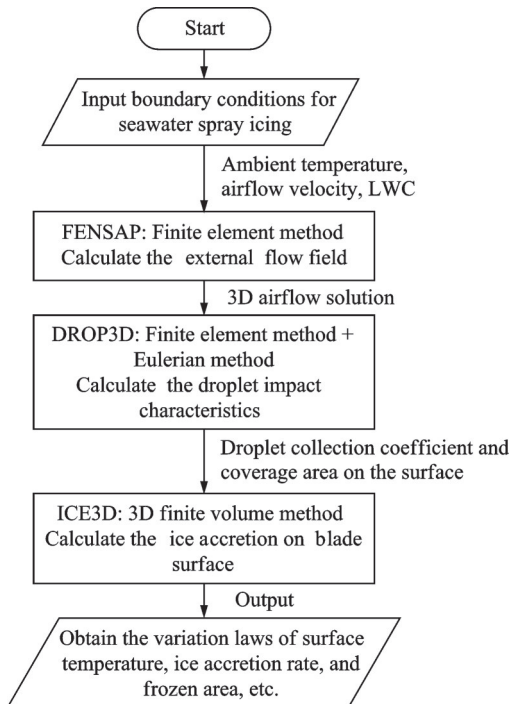


Fig.7 Flow chart of spray impingement and icing calculation

lation yields the air velocity and pressure distributions, as shown in Fig.8 and Fig.9, respectively.

Based on the simulation results of the air flow field, it is evident that the pressure at the leading

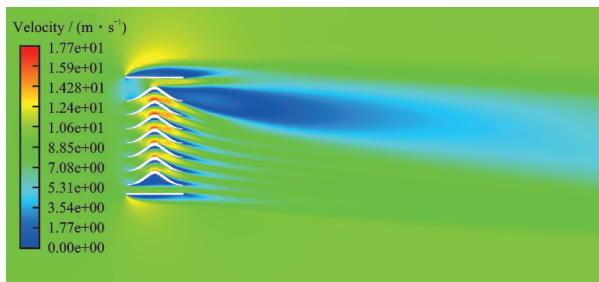


Fig.8 Contour plot of air velocity distribution near the grille

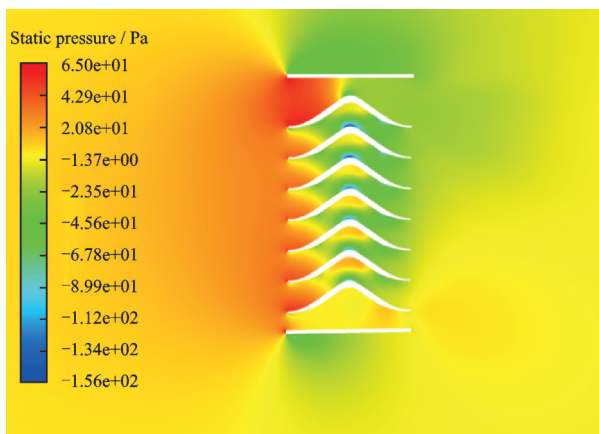


Fig.9 Contour plot of pressure distribution near the grille

edge of the blade is significantly higher. Due to the geometric constraints of blades, the pressure drops sharply as the airflow passes through the grille blades, forming a sheltered region with relatively low velocity. The airflow between the outermost blade and the outer frame of the grille is significantly influenced by compression and expansion effects, resulting in a relatively large sheltered region.

2.1 Grid independence study

Before conducting the impingement characteristics analysis of droplets and the icing analysis, a quantitative mesh independence study must first be performed. For the ship intake grille, three sets of flow field grids with different mesh densities are constructed, all utilizing structured grids. The total number of grids are 3.06, 4.24, and 7.72 million, respectively.

As shown in Fig.10, the droplet collection coefficient curves on the surface of the central blade are presented for three different sets of grids under the conditions of an ambient temperature of $-20\text{ }^{\circ}\text{C}$, a LWC of 8 g/m^3 , and a MVD of $50\text{ }\mu\text{m}$. In the horizontal axis, x represents the position along the blade surface, while c denotes the total chord length of the blade.

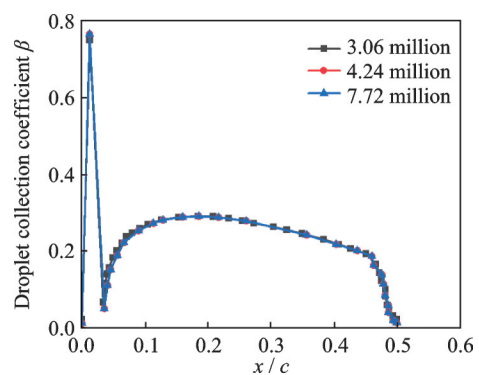


Fig.10 Droplet collection coefficient curves for different sets of grids

The droplet impingement characteristics calculated under the same operating conditions are essentially consistent across different grid sizes. Therefore, for subsequent analysis in this study, a computational model with a grid size of 4.24 million cells is adopted.

2.2 Analysis of droplet impingement characteristics

During the navigation of a ship, supercooled water droplets impinge on the grille surfaces, forming an impingement zone. The size of this zone and the distribution of the impingement water mass are referred to as droplet impingement characteristics, which constitute an indispensable and critical step prior to icing calculations.

To investigate the quantitative influence of MVD values on the droplet impingement characteristics, a comparative analysis is conducted under conditions with a temperature of $-20\text{ }^{\circ}\text{C}$ and a LWC of 8 g/m^3 . During the calculation, the inlet droplet diameter is assumed to be uniform, and the droplet temperature is maintained consistent with the airflow. Since the droplet diameters used in the study are relatively large, the influence of gravity is taken into account in the calculation.

For analytical clarity, the protruding side and recessed side of blades are illustrated as follows. For each blade, the left side as shown in Fig.11 is defined as the protruding side, and the right side is defined as the recessed side. Both sides of the blade consist of a windward surface and a leeward surface.

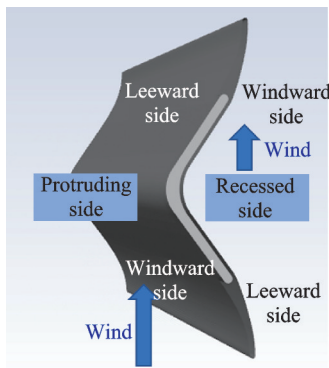


Fig.11 Schematic diagram of the blade structure

Taking a case of $\text{MVD}=50\text{ }\mu\text{m}$ as an example, Fig.12 shows the contour of droplet collection coefficient on the grille surface, with the airflow direction being in the x direction.

Further investigation into the influence of droplet MVD on droplet impingement characteristics on the surface is conducted, with a comparative analysis focusing on the central blade. Fig.13 illustrates the contour map of droplet collection coefficients on



Fig.12 Overall contour of droplet collection coefficient on the grille surface at $\text{MVD}=50\text{ }\mu\text{m}$, $t_a=-20\text{ }^{\circ}\text{C}$, and $\text{LWC}=8\text{ g/m}^3$

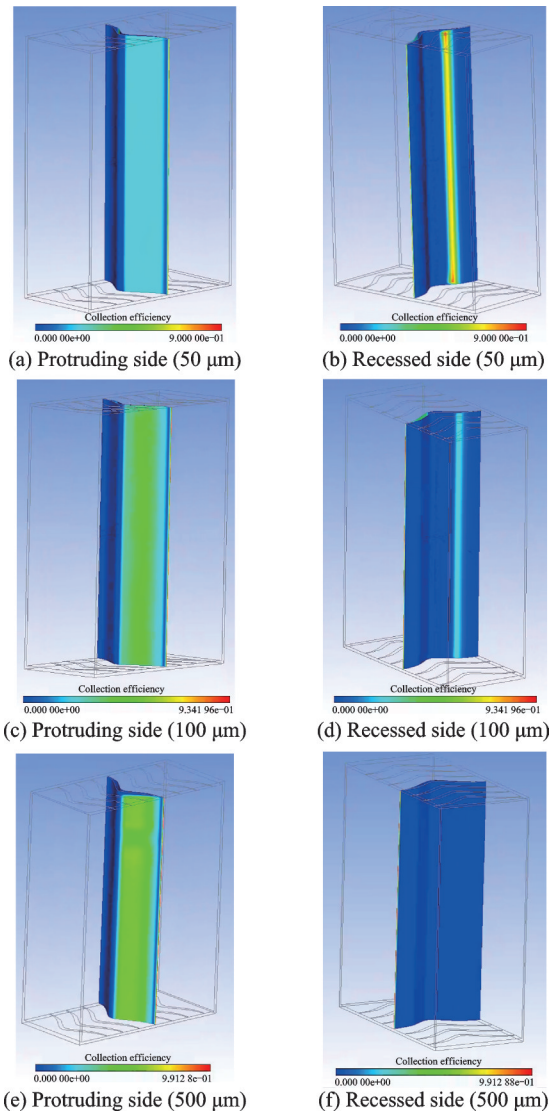


Fig.13 Contour of droplet collection coefficients on the surface of the central blade for MVD ranging from $50\text{ }\mu\text{m}$ to $500\text{ }\mu\text{m}$ at $t_a=-20\text{ }^{\circ}\text{C}$ and $\text{LWC}=8\text{ g/m}^3$

the surface of the central blade for MVD ranging from $50\text{ }\mu\text{m}$ to $500\text{ }\mu\text{m}$.

The analysis of Figs.13(a) and (b) reveals a

strong positive correlation between the mass of impingement water and the windward area. The leading edge of blades tends to accumulate more water upon impact. Due to the influence of blade's geometric configuration, on the protruding side of the blade, the mass of impinged water initially increases and then decreases with the change of the frontal area, while the leeward side exhibits almost no water impingement. On the recessed side, there is a possibility that the water droplets may produce some impact at the rear as the airflow is affected by the geometry of the blades.

A comparison of images in Fig.13 reveals that as the droplet diameter increases, the range of water droplet impact on the windward side of the protruding blade remains largely unchanged, while the collection on the recessed side shows significant differences. For small particle sizes ($MVD=50\ \mu\text{m}$), droplets form a dual-peak impact zone at the front region of the protruding side and the rear region of the recessed side. However, as the particle size increases, the amount of water collected on the recessed side decreases progressively. When the MVD reaches $500\ \mu\text{m}$, the impact zone contracts to the front region of the protruding side. This indicates that the distribution range of impacting water varies with the droplet size, which provides valuable guidance for the design of experimental conditions.

2.3 Comparative analysis of icing simulation

The LWC is varied within the range of 0.5/1/2/4/8 g/m^3 , the ambient temperature is varied within the range of $-20/-12/-4\ ^\circ\text{C}$, and the MVD is varied within the range of 50/100/200/500 μm .

Fig.14 shows contours of the icing rate on the grille surface at $t_a = -20\ ^\circ\text{C}$, $MVD=50\ \mu\text{m}$, and $LWC=8\ \text{g}/\text{m}^3$. It is observed that when the droplet diameter is small, significant icing occurs on both sides of the blade, including the front region of the protruding side and the rear region of the recessed side. This result is consistent with the analysis of droplet impingement characteristics.

To comprehensively understand the icing phenomenon under various meteorological conditions, the environmental temperature, MVD, and LWC are taken as variables. The maximum icing rate within the flow channel on the blade surface, which

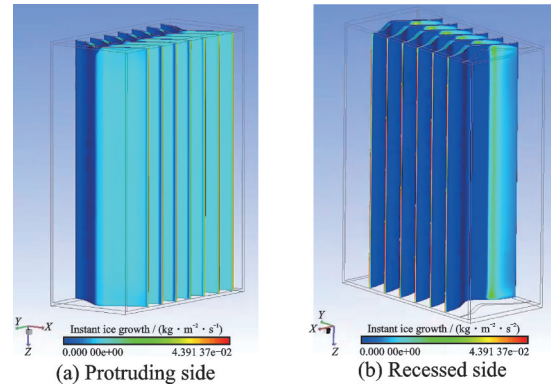


Fig.14 Contours of icing rate on the grille surface at $t_a = -20\ ^\circ\text{C}$, $MVD=50\ \mu\text{m}$, and $LWC=8\ \text{g}/\text{m}^3$

best characterizes the degree of flow channel blockage due to icing, is used to simply assess the icing severity. It can be seen from Fig.15 that when the

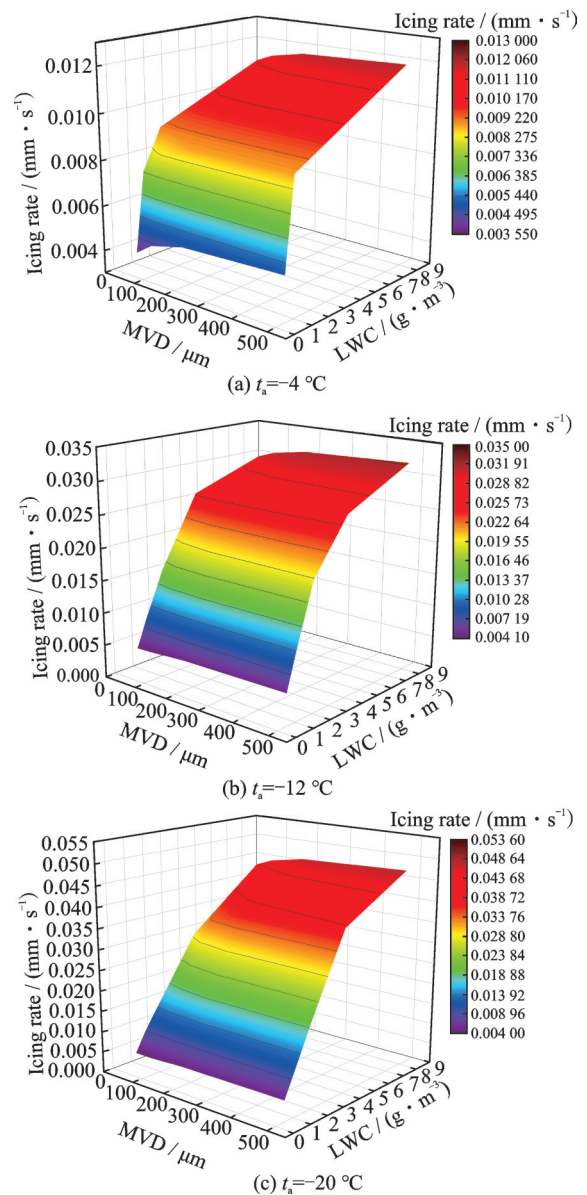


Fig.15 Diagrams of icing rate patterns on grille surface

temperature is low and the liquid water content is high, the icing rate on the grille surface is higher. Droplet diameter has a relatively small effect on the maximum icing rate, but affects the spatial distribution of ice, which is consistent with simulation results of droplet impingement characteristics.

Under the most severe conditions, with a temperature of $-20\text{ }^{\circ}\text{C}$, a droplet diameter of $500\text{ }\mu\text{m}$, and a liquid water content of 8 g/m^3 , the ice thickness can reach 1.176 mm in 1 min . If icing continues for 10 min , and given that the blade spacing is 38.0 mm , the blockage ratio is calculated as $11.76/38.0 \times 100\% = 30.95\%$.

3 Anti-icing Strategy Evaluation

3.1 Uniform heating strategy evaluation

Thermal ice protection systems are currently the most widely used ice protection systems. This paper evaluates the anti-icing system of the ship intake grille based on electro-thermal heating. Building on the simulation of spray icing, an in-depth technical analysis of new anti-icing scheme is conducted according to the designed electric heating architecture and control strategy. The quantitative impact of component heating on the anti-icing performance under various spray icing conditions is further evaluated. The simulation calculation flowchart is shown in Fig.16.

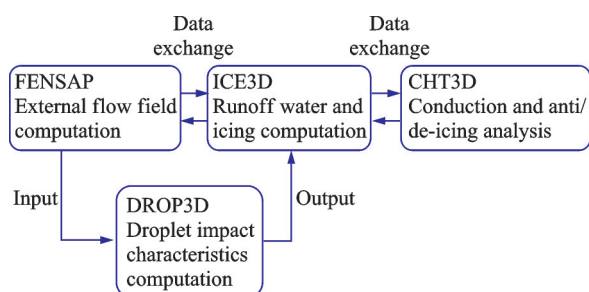


Fig.16 Flowchart of anti-icing simulation

Taking the calculation condition of $-20\text{ }^{\circ}\text{C}$ temperature, $50\text{ }\mu\text{m}$ droplet diameter, and 8 g/m^3 liquid water content as an example, an optimal electric heating strategy is studied. For each blade, the arrangement of the heating film is shown in Fig.17, with coverage only on the upper sidewall of the blade cavity.

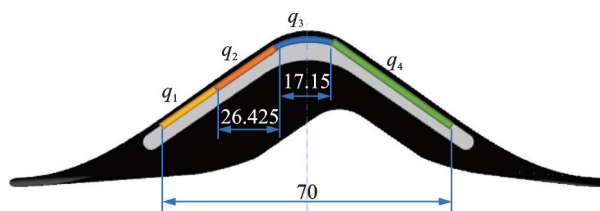


Fig.17 Arrangement of the heating film

Traditional anti-icing systems on ships adopt a completely uniform heating film, meaning that the surface heat flux density is consistent across all heating zones. When $q_1 = q_2 = q_3 = q_4 = 31\,200\text{ W/m}^2$ in Fig.17, although ice formation in the flow channel can be suppressed, residual ice still exists at the leading edge of the blade, with a maximum icing rate of approximately $0.027\text{ kg}/(\text{m}^2 \cdot \text{s})$, as shown in Fig.18(a). Additionally, there is a significant temperature difference on the surface. The maximum surface temperature of the blade is $67.62\text{ }^{\circ}\text{C}$, located in the central region of the blade, as shown in Fig.18(b). This indicates that a uniform heating

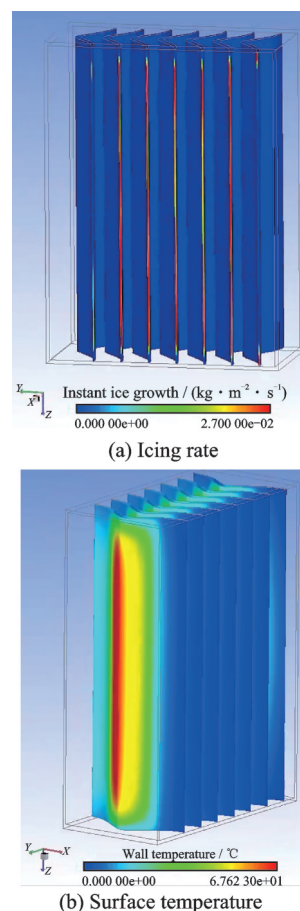


Fig.18 Contours of anti-icing performance under uniform heating strategy of $q_1 = q_2 = q_3 = q_4 = 31\,200\text{ W/m}^2$

power cannot adequately meet the anti-icing requirements and results in heat wastage instead.

3.2 Heating strategy optimization

Based on the calculation results, a zoned heat-

ing scheme is proposed, where the high-power zone at the leading edge and the low-power zone at the center work in synergy. Several heating modes are designed, and the calculation results are summarized in Table 2.

Table 2 Cases for anti-icing simulation

Serial number	Heating power/(W·m ⁻²)	Maximum surface temperature t_{\max} /°C	Icing rate in flow channel/(kg·m ⁻² ·s ⁻¹)	Total heating power consumption/W
1	$q_1 = q_2 = q_3 = q_4 = 31\,200$	67.62	0	1 107.66
2	$q_1 = 45\,000, q_2 = 30\,000,$ $q_3 = 15\,000, q_4 = 30\,000$	61.34	0	1 051.77
3	$q_1 = 20\,000, q_2 = 20\,000,$ $q_3 = 0, q_4 = 20\,000$	24.03	0.038 89	554.13
4	$q_1 = 25\,000, q_2 = 25\,000,$ $q_3 = 0, q_4 = 22\,000$	41.41	0.003 6	651.11
5	$q_1 = 20\,000, q_2 = 20\,000,$ $q_3 = 0, q_4 = 25\,000$	45.31	0	692.66

By comparing working conditions 1 and 2, it can be observed that the heating power in zone 1 has increased from 31 200 W/m² to 45 000 W/m², but residual icing still persists at the blade leading edge. This indicates that the cost of increasing the heat flux density in this zone to elevate the tip temperature is relatively high. Since the icing at the blade leading edge grows forward and has a minor impact on flow channel blockage, the optimization of the heating strategy focuses primarily on the icing within the flow channel, sacrificing the anti-icing performance at the blade leading edge to significantly reduce the power consumption of the anti-icing system. To further enhance the anti-icing performance at the blade leading edge, an optimized design of the blade geometry is required.

In response to the significant surface temperature differences observed, the heating power for the four zones is optimized. Based on working condition 2, the electric heating power for each zone is reduced, resulting in working conditions 3 and 4. It is found that the maximum surface temperature decreases significantly, but partial icing occurs within the flow channel, which does not meet the anti-icing requirements. Therefore, the heating power for zone 4 should be increased, resulting in working condition 5. Comparing the uniform heating power

condition (working condition 1) with the optimized condition (working condition 5), it is evident that while meeting the anti-icing requirements, the maximum surface temperature decreases from 67.62 °C to 45.31 °C, and the total power consumption is reduced by $(1\,107.66 - 692.66)/1\,107.66 \times 100\% = 37.47\%$.

Thus, to address the spray icing phenomenon encountered during ship navigation in cold conditions, a zoned electric heating approach should be adopted for intake grilles. Precise distribution of heat flux can significantly optimize the anti-icing performance and reduce electric heating energy consumption.

4 Conclusions

This study constructs a three-dimensional model of the ship power intake grille and systematically reveals the droplet impact characteristics and icing dynamics of spray. It quantitatively investigates the influence of environmental temperature, droplet diameter, and liquid water content on flow channel blockage. The results indicate that: (1) Environmental temperature and liquid water content are the dominant factors affecting the icing rate. Under the most severe conditions of -20 °C and a liquid water content of 8 g/m³, the flow channel blockage ratio

can reach 30.95% after 10 min. (2) Droplet diameter alters the water impact distribution characteristics on the blade surface, thereby influencing the ice layer morphology. Small-diameter droplets (50 μm) form a dual-peak impact zone at the front region of the protruding side and the rear region of the recessed side, while large-diameter droplets (500 μm) are concentrated in the impact zone on the protruding side.

Based on these findings, a zoned electric heating anti-icing optimization strategy is proposed. Through coordinated control, while ensuring the anti-icing effect in the flow channel, the maximum surface temperature is reduced from 67.62 $^{\circ}\text{C}$ to 45.31 $^{\circ}\text{C}$, and the total power consumption is decreased by 37.47%, demonstrating significant advantages of the proposed strategy in reducing thermal load and energy consumption.

By delving into the icing and anti-icing mechanisms of spray impingement on the ship's grille, this study provides critical data support for the safe operation of ship power systems in cold sea areas. Future work will combine experimental validation and multi-physical field coupling models to further optimize the engineering applicability of the anti-icing system.

In addition, in the future work, we will further investigate the impact of seawater salinity on the freezing rate.

References

- [1] BORISENKOV E P. Investigation of the physical nature of ship icing: CRREL-TL-411[R]. Hanover, USA: U.S. Army Cold Regions Research and Engineering Laboratory, 1974.
- [2] TABATA T. Studies on the ice accumulation on ships. III. Relation between the rate of ice accumulation and air, sea conditions[J]. *Low Temperature Science. Series A, Physical Sciences*, 1970, 27: 339-349.
- [3] MINSK L D. Ice accumulation on ocean structures: CRREL-77-17[R]. Hanover, USA: U. S. Army Cold Regions Research and Engineering Laboratory, 1977.
- [4] EFIMOV Y, KORNISHIN K. Vessel icing on the Shtokman FPSO[C]//Proceedings of OTC Arctic Technology Conference. Houston, USA: [s.n.] , 2012: OTC-23718-MS.
- [5] SAWADA T. Ice accretion on ships in northern seas of Japan[J]. *Journal of the Meteorological Society of Japan*, 1968, 46(3): 250-254.
- [6] MERTINS H O. Icing on fishing vessels due to spray[J]. *Marine Observer*, 1968, 38(221): 128-130.
- [7] WALSH M R, GARFIELD D E, MORSE J S, et al. Icing of turbine intake louvers[R]. Hanover, USA: U.S. Army Cold Regions Research and Engineering Laboratory, 1993.
- [8] RYERSON C C. Superstructure spray and ice accretion on a large U. S. Coast Guard cutter[J]. *Atmospheric Research*, 1995, 36(3/4): 321-337.
- [9] MINTU S, MOLYNEUX D. Ice accretion for ships and offshore structures. Part 2—Compilation of data[J]. *Ocean Engineering*, 2022, 248: 110638.
- [10] MAKKONEN L. Heat transfer and icing of a rough cylinder[J]. *Cold Regions Science and Technology*, 1985, 10(2): 105-116.
- [11] PAUL ZAKRZEWSKI W, LOZOWSKI E P, MUGGERIDGE D. Estimating the extent of the spraying zone on a sea-going ship[J]. *Ocean Engineering*, 1988, 15(5): 413-429.
- [12] BLACKMORE R Z, LOZOWSKI E P. An heuristic freezing spray model of vessel icing[J]. *International Journal of Offshore and Polar Engineering*, 1994, 4(2): ISOPE-I-93-196.
- [13] KULYAKHTIN A, TSARAU A. A time-dependent model of marine icing with application of computational fluid dynamics[J]. *Cold Regions Science and Technology*, 2014, 104: 33-44.
- [14] KULYAKHTIN A, KULYAKHTIN S, LØSET S. The role of the ice heat conduction in the ice growth caused by periodic sea spray[J]. *Cold Regions Science and Technology*, 2016, 127: 93-108.
- [15] SAMUELSEN E M, EDVARDBEN K, GRAVERSEN R G. Modelled and observed seaspray icing in Arctic-Norwegian waters[J]. *Cold Regions Science and Technology*, 2017, 134: 54-81.
- [16] HORJEN I. Modeling of icing on a planar surface due to sea spray and blowing snow[J]. *Ocean Engineering*, 2023, 285: 115339.
- [17] DESHPANDE S, SÆTERDAL A, SUNDSBØ P A. Experiments with sea spray icing: Investigation of icing rates[J]. *Journal of Offshore Mechanics and Arctic Engineering*, 2024, 146(1): 011601.

Acknowledgement This work was supported in part by the Ship Preliminary Research Project (No.3020401020102).

Authors

The first author Ms. FENG Huiying received the B.S. degree from School of Mechanical Engineering in Yantai University in 2005. She joined Systems Engineering Research Institute of CSSC in 2020, where she currently served as a product development engineer. Her main research interest is the development of protective equipment for ship power intake and exhaust systems.

The corresponding author Mr. PAN Tao received his B.S. and M.S. degrees in naval architecture and ocean engineering, and design and manufacturing of ships and marine structures from Harbin Engineering University in 2007 and 2010, respectively. In the same year, he joined the Systems Engineering Research Institute of CSSC, where he currently

serves as a researcher. His research focuses on the design and technical studies of protective equipment for ship power systems.

Author contributions Dr. BU Xueqin designed the models and revised the manuscript. Ms. FENG Huiying provided the simulation resources and wrote the manuscript. Mr. PAN Tao designed the blade model and processed some simulation data. Ms. LOU Yanxia performed the simulation calculations. All authors commented on the manuscript draft and approved the submission.

Competing interests The authors declare no competing interests.

(Production Editor: WANG Jing)

寒环境下船舶进气口格栅飞沫结冰与防除冰仿真研究

冯慧英¹, 潘涛¹, 楼燕霞², 卜雪琴²

(1. 中国船舶集团有限公司系统工程研究院, 北京 100094, 中国; 2. 北京航空航天大学航空科学与工程学院, 北京 100191, 中国)

摘要:研究了寒冷海洋环境中船舶动力系统进气格栅的海水飞沫结冰问题。通过数值模拟方法,揭示环境参数对结冰特性的影响,并提出了一种更节能的分区电加热防冰策略。通过构建一个三维格栅模型,系统分析了环境温度(-20至-4℃)、液滴直径(50至500 μm)和液态水含量(0.5至8 g/m³)对结冰速率和流道堵塞的影响。结果表明,低温和高液态水含量显著加剧了结冰。在环境温度为-20℃、液滴直径为500 μm、液态水含量为8 g/m³的条件下,流道堵塞率在10 min内达到了30.95%。此外,随着液滴直径的增加,液滴撞击和结冰区域更加集中在叶片的前缘。为了缓解寒冷环境中的格栅结冰问题,通过布置电加热膜的方式来进行电热防护。通过将表面加热膜分区优化布置,优化后的加热策略与初始的均匀加热方案相比,能够有效均匀化表面温度分布,同时将总功耗降低了37.47%。本研究验证了分区电加热防冰/除冰策略的工程适用性,为寒冷海洋区域船舶动力系统防冰系统的设计提供了理论和技术支持。

关键词:船舶进气格栅;结冰特性;海洋环境;流道堵塞;分区电加热策略